

# GRAPHITE: A Practical Framework for Generating Automatic Physical Adversarial Machine Learning Attacks

Ryan Feng<sup>1</sup>, Neal Mangaokar<sup>1</sup>, Jiefeng Chen<sup>2</sup>, Earlence Fernandes<sup>2</sup>, Somesh Jha<sup>2</sup>, Atul Prakash<sup>1</sup>

<sup>1</sup>University of Michigan, Ann Arbor, <sup>2</sup>University of Wisconsin, Madison

<sup>1</sup>{rtfeng, nealmgkr, aprakash}@umich.edu, <sup>2</sup>{jiefeng, earlence, jha}@cs.wisc.edu

**Abstract**—This paper investigates an adversary’s ease of attack in generating adversarial examples for real-world scenarios. We address three key requirements for practical attacks for the real-world: 1) *automatically* constraining the size and shape of the attack so it can be applied with stickers, 2) *transform-robustness*, i.e., robustness of a attack to environmental *physical* variations such as viewpoint and lighting changes, and 3) supporting attacks in both white-box and black-box *hard-label* scenarios, so that the adversary can attack proprietary models. In particular, the art of automatically picking which areas to perturb remains largely unexplored — an efficient solution would remove the need to search over possible locations, shapes, and sizes as in current patch attacks. In this work, we propose GRAPHITE, an efficient and general framework for generating attacks that satisfy the above three key requirements. GRAPHITE takes advantage of transform-robustness, a metric based on expectation over transforms (EoT), to *automatically* generate small masks and optimize with gradient-free optimization. GRAPHITE is also flexible as it can easily trade-off transform-robustness, perturbation size, and query count in black-box settings. On a GTSRB model in a hard-label black-box setting, we are able to find attacks on all possible 1,806 victim-target class pairs with averages of 77.8% transform-robustness, perturbation size of 16.63% of the victim images, and 126K queries per pair. For digital-only attacks where achieving transform-robustness is not a requirement, GRAPHITE is able to find successful small-patch attacks with an average of only 566 queries for 92.2% of victim-target pairs. GRAPHITE is also able to find successful attacks using perturbations that modify small areas of the input image against PatchGuard, a recently proposed defense against patch-based attacks.

**Index Terms**—adversarial examples, patch attacks, physical attacks, black-box attacks, graphite

## 1. Introduction

Machine learning (ML) models have had resounding success in several scenarios such as face and object recognition [1]–[5]. Therefore, such models are now a part of perception pipelines in cyber-physical systems like cars [6]–[8], UAVs [9], [10] and robots [11]. However, recent work has found that these models are vulnerable to subtly perturbed adversarial examples that cause misclassification [12]–[15]. While these early digital white-box attacks were useful in understanding model weaknesses, researchers are now considering how to make attacks

more practical for adversaries to accomplish in the real world [16]–[21].

Practical, real-world attacks have three key requirements. The first is that they should *automatically* choose small areas to perturb, so that they can be applied with stickers on existing physical objects. The second is that practical, real-world attacks should exhibit *transform-robustness*, i.e., be robust to *physical*-world effects such as viewpoint and lighting changes as measured by a metric based on expectation over transforms [16]. The final requirement is that the most powerful real-world attacks should only require *hard-label* access. This means that the adversary can succeed with only the final top-1 decision, which *must* be provided by a deployed ML model for it to be useful even if its internals are closed source and designed to be difficult to completely reconstruct due to proprietary formats, implementations, and stripped binaries [22]. The adversary should also be able to work with smaller query budgets when that is a constraint.

Regarding the first requirement, the art of *automatically* picking limited areas to perturb remains relatively unexplored. Existing patch attacks [17], [23]–[26] limit perturbations to small patches, but are restricted to pre-defined patch shapes. The adversary must also either search for a good location and size, or optimize over an expectation of patch locations and sizes. This is inefficient and, in black-box settings, query-intensive. Existing work also shows that targeted attacks require larger patches [26].  $RP_2$  [18] uses masks to constrain the space of the attack, but the mask creation process requires some manual experimentation, making it harder to scale. The Carlini & Wagner  $\ell_0$  attack [12] generates arbitrary, small sets of pixels to perturb, but is designed for digital attacks, not for physical settings or where only hard-label access to a model is available (requirements 2 and 3).

Likewise, existing work on finding attacks in the hard-label case do not satisfy the first two requirements; instead, they find digital attacks that require tens or hundreds of thousands of queries [20], [21], [27], [28].

We generalize these principles and *combine all three requirements* for the first time, to our knowledge, creating a more practical and efficient real-world attack framework called GRAPHITE (Generating Robust Automatic Physical Image Test Examples). Such an attack framework could be potentially useful for security testing of and improving future defenses. We formulate our automatic framework of physical attacks as a joint optimization problem, balancing the opposing goals of minimizing perturbation size (or “mask size”) and maximizing transform-robustness. More broadly, the framework is designed to

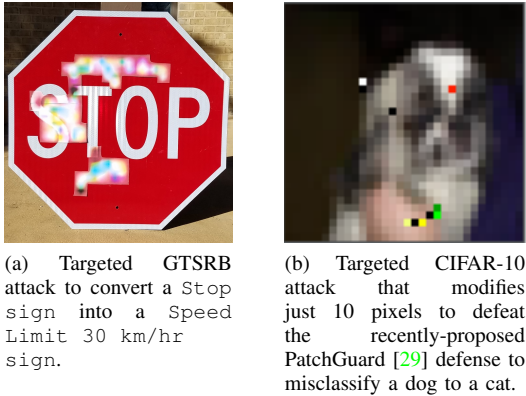


Figure 1. Example GTSRB and CIFAR-10 GRAPHITE-generated black-box hard-label attacks.

find attacks that permit tradeoffs among different constraints of query budgets (in hard-label settings), mask size, and transform-robustness.

We first instantiate this framework in the white-box setting by adapting Carlini Wagner’s  $\ell_0$  attack [12] to help satisfy the three requirements. We show that the resulting attacks require a nearly 2x lower number of forward/backward passes compared to typical square patch attacks, and also exhibit more transform-robustness.

We then propose an instantiation of the framework for the more challenging hard-label setting. We show that there are significant algorithmic differences between the white-box and black-box attacks that are motivated by the general difficulties of naïve  $\ell_0$  style minimization attacks in the highly discrete and discontinuous hard-label optimization space. As a result, we show experimentally that simply extending white-box attacks to hard-label black-box settings using strategies such as OPT [20] yields poor results in Section 5.1. We solve these challenges by separating the joint optimization into a two stage approximation: automatic mask generation and perturbation boosting, while using transform-robustness to provide a more continuous measure (as compared to just success or failure of an attack) to determine the relative value of keeping or removing pixels.

We evaluate our GRAPHITE framework in hard-label black-box settings on all 1,806 victim-target pairs of German Traffic Sign Recognition Benchmark (GTSRB) classes, additionally restricting the attack to be contained within the victim object boundaries for physical sticker potential. We achieve an average transform-robustness of 77.8% and an average mask size of 16.63% of the victim image with 126k queries. As this is the first physical hard-label attack, we also verify results in the physical-world with 420 field test images in the form of stickers on real-world objects (including a successful Speed Limit 30 km/hr sign attack in 201 / 210  $\approx$  95.7% images). We then demonstrate our framework’s ability to trade off mask size, transform-robustness, and query count. In one such setting, when transform-robustness is not required or low values suffice, GRAPHITE is able to find successful small-patch attacks for over 92.2% of GTSRB victim-target pairs with just 566 queries per successful pair. In contrast, state-of-the-art hard-label attacks of any type (including those bounded by  $\ell_2$  or  $\ell_\infty$  norms) on similar

datasets all report requiring tens to hundreds of thousands of queries, i.e., one to three orders of magnitude higher.

Finally, to demonstrate GRAPHITE’s ability to *thwart existing defenses*, we select a state-of-the-art patch attack defense called PatchGuard [29] and attack a defended CIFAR-10 model in the hard-label black-box setting. Across 50 random victim-target image pairs, we are able to successfully attack PatchGuard by perturbing as little as 1% of the pixels (e.g., see Figure 1b). This also demonstrates the value of a framework that can generate more generalized forms of patch attacks (e.g., attacks using multiple patches) than those considered by PatchGuard; PatchGuard primarily evaluated its scheme on patches in a single part of an image.

## Our Contributions:

- We proposed a general framework for generating practical, real-world attacks that combine three key requirements (that they are *automatically* space constrained, *physically* robust to transformations, and only require black-box *hard-label* access). The algorithms based on the framework generate attacks efficiently in both white-box and black-box settings.
- We introduce the first automatic, robust physical perturbation attacks in the black-box hard-label setting. We presented a novel mask generation process that *automatically* generates candidate masks to constrain the perturbation size and showed that transform-robustness is a sufficiently smooth function to optimize with gradient-free optimization.
- We demonstrated GRAPHITE’s ability to trade off transform-robustness, query budget, and mask size depending on the adversary’s limitations and priorities. As an example, we generate attacks with non-negligible transform-robustness in 92.2% of GTSRB victim-target pairs with an average of just 566 queries and an average mask size of 10.5%.

## 2. Related Work

**Automatic Attacks.** The art of constraining the size and shape of perturbations remains relatively unexplored. One approach to limit the perturbation size is to use a patch attack. Patch attacks were first proposed as a white-box technique that crafted small perturbation patches that could be added to any scene to cause a misclassification [17]. Later work then explored patch attacks on object detection [23], [24] and the soft-label setting [25], [26], where the model output probabilities are available. Oftentimes, the patches are made robust to different spatial locations by optimizing over different patch locations. However, these approaches must run inferences over many locations and are stuck to static shapes. In contrast, we are able to efficiently generate arbitrarily-shaped perturbations and do so with only hard-label access, where only the top-1 class prediction is known.

Other work that limits the size of perturbation includes RP<sub>2</sub> [18], a physical white-box attack that designs adversarial stickers and the Carlini-Wagner (C&W)  $\ell_0$  attack [12]. RP<sub>2</sub> introduces the notion of a *mask* to limit the size of the perturbation. However, their process requires some manual experimentation based on the visual results

of an  $\ell_1$  approximation. The C&W  $\ell_0$  attack alternates between pixel removal and the C&W  $\ell_2$  attack to optimize an  $\ell_0$ , but is designed for digital white-box setting, failing to meet requirements 2 and 3.

**Physical Attacks.** Existing work for robust physical perturbation attacks on image models remains in the *white-box* setting. Examples include printing images of perturbed objects [30], modifying objects with stickers [18], [19], and 3D printing perturbed objects [16]. Such attacks typically optimize the expectation over a distribution of transformations, known as *Expectation over Transformation (EoT)* [16]. Such transformations model changes in viewing angle, distance, lighting, etc. In this work, we describe the expectation of attack success over such transformations as the *transform-robustness* of an attack, approximated by measuring the attack success rate with some number of transformations. Some attacks also introduce the notion of a mask that constrains the perturbation to small regions of the object [18]. However, existing work does not fully automatically generate suitable masks, and the mask is not jointly optimized with the noise.

In contrast, we automatically generate small masks to confine perturbations. Additionally, we extend our construction of such attacks to the blackbox hard-label setting.

**Black-box Attacks.** Recent work has explored *digital* hard-label attacks [20], [21], [27], [28], [31], where only the top-1 label prediction is available. Such attacks are difficult because the hard-label optimization space is discontinuous and discrete. One approach is to reformulate the objective into a continuous optimization problem that finds the perturbation direction at which the decision boundary is closest. This approach is taken by OPT-attack [20], which uses the Randomized Gradient Free (RGF) method [32], [33] to optimize this distance-based objective. The boundary distance is calculated through a binary search process. The perturbation is initialized by interpolating with a target class image.

In our work, we generate physically robust examples within small masked areas with only hard-label access. As we show in Section 5.1, directly adding EoT to this distance-based reformulation is both inefficient and ineffective, leaving visible artifacts of the intended target. Unlike OPT-attack, we also generate masks.

Other black-box work includes transfer and soft-label attacks. Transfer attacks train a surrogate model, generate white-box examples on the surrogate, and hope they transfer to the target [34]. Unfortunately, targeted examples often fail to transfer [35]. Many techniques also require access to similar training sets that may not be available, whereas our work only requires query access to the target model. Soft-label attacks, or *score-based* attacks, require access to the softmax layer output in addition to class labels [36], [37]. In contrast, our threat model only allows the adversary top-1 predicted class label access.

### 3. Setting up Automatic Physical Attacks

In this section, we lay the groundwork for our general joint optimization problem for automatic physical attacks. We define automatic physical attacks to be ones that: 1) automatically pick a small mask consisting of pixels to perturb and 2) are robust to some set of transformations, set to model environmental variation such as viewpoint

and lighting changes. We then show that mask generation is an NP-complete problem.

### 3.1. Problem Setup

Our goal is to find some perturbation  $\delta$  and a small mask  $M$  such that when  $\delta$  is applied to a victim image  $x$  in the area defined by mask  $M$ , our model  $F$  predicts the target label  $y_{tar}$  with high transform-robustness. Transform-robustness is estimated over  $t$  transforms sampled from a distribution of transforms  $T$ . We describe a targeted attack formulation, but can easily adapt to untargeted.

### 3.2. Optimizing Mask and Transform-robustness

The optimal perturbation maximizes transform-robustness (i.e., EoT metric) while occupying only a small area of the object such as a traffic sign.  $M_{ij}$  is 1 if pixel at position  $(i, j)$  is perturbed and 0 otherwise. A way to model such constrained optimization problems is to model it as a joint optimization problem, which we give below.  $\lambda > 0$  is the relative weight given to size of the mask  $M$  in the joint objective:

$$\operatorname{argmin}_{\delta, M} \lambda \cdot \|M\|_0 - \mathbb{E}_{t \sim T} \left[ F \left( t(x + M \cdot \delta) \right) = y_{tar} \right] \quad (1)$$

where the second term is defined as *transform-robustness*, computed as an expectation of attack success rate. In practice, we estimate this with a set of randomly sampled transforms. We observe that directly solving this objective is generally challenging, especially in the hard-label setting as we see in Section 5. Furthermore, the problem of finding an optimal solution with a constrained mask size is NP-complete, as we prove in Appendix A. One approach to constructing such masks is to adopt an  $\ell_0$  “heuristic” (the  $\ell_0$  norm itself is fundamentally non-differentiable, so straightforward adaptations of gradient descent or OPT-attack cannot be used). As an example, JSMA [14] builds a mask by considering the pixels most “relevant” towards causing a misclassification and Carlini and Wagner’s  $\ell_0$  attack [12] reduces a mask by removing least “relevant” pixels; both approaches require doing a large number of forward passes over the model (e.g., a pass for each pixel) to find most relevant or least pixel, since the problem is non-differentiable. This forward-pass method works in the white-box setting, but, as further discussed in Section 5, does not work in the hard-label setting where logits are not available; changing a pixel is unlikely to change the classification result, making it challenging to identify most relevant or least relevant pixels.

### 3.3. General Algorithmic Pipeline

For reducing mask size and increasing transform-robustness, we describe the general GRAPHITE solver framework with pseudocode in Algorithm 1. As the  $\ell_0$  norm inherently makes (1) difficult to solve directly, we alternate between reducing the mask size and improving the attack with the set of perturbable pixels. The framework first initializes a perturbation and gradient, and then iteratively selects pixels to remove, removes them, and

attacks the remaining pixels. This process is repeated until a specified stopping criteria is met. In order to work well, the framework generally requires an inner attack to find transform-robust attacks and a way to order pixels.

---

#### Algorithm 1 General GRAPHITE Framework

**Input:** Victim Image  $x$ , Target Image  $x_{tar}$ , Initial Mask  $M_{init}$ , Model  $F$ , Target Label  $y_{tar}$   
**Output:** Attacked Image  $A$ , Mask  $M$ , Perturbation  $\delta$

- 1:  $M \leftarrow M_{init}$
- 2:  $\delta, g \leftarrow \text{INIT\_PERT\_+\_GRAD}(x, x_{tar}, M, F, y_{tar})$
- 3: **while** not done **do**
- 4:    $S \leftarrow \text{SELECT\_PIXELS}(x, x_{tar}, M, \delta, y_{tar}, g)$
- 5:    $M \leftarrow \text{REMOVE\_PIXELS}(M, S)$
- 6:    $A, \delta, g \leftarrow \text{ATTACK}(x, x_{tar}, M, \delta_{init}, F, y_{tar})$
- 7: **end while**
- 8:  $A, \delta \leftarrow$  Last Successful Attack

---

## 4. White-box Automatic Physical Attacks

In this section, as an implementation of the GRAPHITE framework in Algorithm 1, we extend the Carlini Wagner  $\ell_0$  attack [12] to generate attacks in the white-box setting that have high transform-robustness.

### 4.1. White-box Attack Algorithm

Based on the general GRAPHITE framework, we first aim to create an automatic, physical attack in the white-box setting. To this end, we design an attack inspired by the Carlini-Wagner (C&W)  $\ell_0$  attack [12]. The original C&W  $\ell_0$  algorithm, as presented in Algorithm 2, fits into our framework. Specifically, the original algorithm greedily reduces the cardinality of the mask (allowed set of pixels that can be perturbed), alternating between pixel removal and running an inner C&W  $\ell_2$  attack until the attack can no longer find an adversarial example. The attack removes the pixel with the least impact, measured by multiplying the gradient and the perturbation together.

For our white-box instantiation of GRAPHITE, we need to add the notion of transform-robustness to the attack. Our algorithm’s pseudocode is shown in Algorithm 3. The first change we make is that we add EoT to the inner attack. Then, to make the attack more similar to our later black-box implementation and to increase efficiency, we swap out the inner C&W  $\ell_2$  minimization attack for PGD [38]. Next, for further efficiency and to encourage larger sticker patches (for printing convenience), we remove  $z$  patches of pixels at a time, where each patch is a  $p \times p$  square of pixels. To collect the list of patches, we stride by a step size of  $s$ . Finally, we set the stopping criteria as our EoT PGD attack being unable to find an attack with at least  $tr_{min}$  transform-robustness.

**Experimental Setup.** To test our attack, we run targeted attacks for all victim-target pairs in a varied, 10 class subset of GTSRB: Stop, Speed Limit 30 km / hr, Speed Limit 80 km / hr, Pedestrians, Turn Left Ahead, Yield, Caution, Roundabout, End of Overtaking Limit, Do Not Enter. Foreshadowing our black-box attack, where we want to show dataset independence,

---

#### Algorithm 2 Original C&W $\ell_0$ Attack

**Input:** Victim Image  $x$ , Model  $F$ , Initial Mask  $M_{init}$ , Target Label  $y_{tar}$   
**Output:** Attacked Image  $A$ , Mask  $M$ , Perturbation  $\delta$

- 1:  $M \leftarrow M_{init}$
- 2:  $A, \delta, g \leftarrow \text{C\&W\_}\ell_2\_ATTACK(x, M, F, y_{tar})$
- 3: **while**  $F(A) = y_{tar}$  **do**
- 4:    $S \leftarrow \{\text{argmin}_i g_i \cdot \delta_i\}$
- 5:    $M_{\{Pixels \in S\}} \leftarrow 0$
- 6:    $A, \delta, g \leftarrow \text{C\&W\_}\ell_2\_ATTACK(x, M, F, y_{tar})$
- 7: **end while**
- 8:  $A, \delta \leftarrow$  Last Successful Attack

---



---

#### Algorithm 3 White-box GRAPHITE Attack

**Input:** Victim Image  $x$ , Model  $F$ , Initial Mask  $M_{init}$ , Target Label  $y_{tar}$   
**Output:** Attacked Image  $A$ , Mask  $M$ , Perturbation  $\delta$

- 1:  $M \leftarrow M_{init}$
- 2:  $A, \delta, g \leftarrow \text{EoT\_PGD\_ATTACK}(x, M, F, y_{tar})$
- 3: **while** Transform-Robustness of  $A > tr_{min}$  **do**
- 4:    $S \leftarrow$  set of  $z$  patches with smallest  $g_i \cdot \delta_i$  values
- 5:    $M_{\{Patches \in S\}} \leftarrow 0$
- 6:    $A, \delta, g \leftarrow \text{EoT\_PGD\_ATTACK}(x, M, F, y_{tar})$
- 7: **end while**
- 8:  $A, \delta \leftarrow$  Last Attack with transform-robustness  $> tr_{min}$  if one was found, else first attack

---

we use images outside of the GTSRB dataset. Since we had a real-world Stop Sign available in our lab, we used a photo we took of that physical sign. For all other GTSRB classes, we attack traffic-sign images downloaded from the Internet. The images are  $244 \times 244$ .

**Hyperparameters.** We set  $z = 4$  and  $tr_{min} = 80\%$ . We choose values of  $p$  and  $s$  such that when rounded to the nearest int, the patches consists of the areas that  $4 \times 4$  patches would occupy in the original  $32 \times 32$  input resolution of GTSRBNet at a stride of 2. We compute transform-robustness with 100 transforms. PGD is performed with a step-size of  $2/255$  and a max of 50 iterations per round of patch removal. The perturbation is restricted to be within the pre-defined boundaries of the victim traffic sign (if desired, object boundaries could be detected automatically with a segmentation network). Finally, we apply a random start on PGD with noise between  $[-8/255, 8/255]$ . Details on the specifics of GTSRBNet and the transformations, which mirrors that of the hard-label attack, can be found in Section 6.1 and Appendix B.

**Patch-PGD.** For comparisons sake, we also compared against the popular square patch attack that simply runs Patch-PGD [29], [39] (with EoT) attack over a square patch of  $64 \times 64$  pixels (about 6.88% of the image). Rather than test every possible location, which is expensive, we test the four corners (as in the weaker adversary in [39]) and the center. We ran it with 100 transforms, 200 steps, and a step size of  $4 / 255$ .

**Results.** Table 1 presents the results from our white-box algorithm and the Patch-PGD baseline on all 90 victim-target pairs of the GTSRB subset. These results show that our approach in general finds patches with higher transform-robustness and more efficiently than the strategy of choosing static squares, even when the lat-



Figure 2. Example targeted, white-box automatic, physically-realizable attacks between: Stop, Speed Limit 30 km/hr, Pedestrians, Turn Left Ahead.

---

#### Algorithm 4 Black-box GRAPHITE Attack

---

**Input:** Victim Image  $x$ , Target Image  $x_{tar}$ , Model  $F$ , Initial Mask  $M_{init}$ , Target Label  $y_{tar}$

**Output:** Attacked Image  $A$ , Mask  $M$ , Perturbation  $\delta$

```

1:  $M \leftarrow M_{init}$ 
2:  $\delta \leftarrow M \cdot (x_{tar} - x)$ 
3: for One Iteration do
4:   // Select and Remove Patches (Mask Generation)
5:    $\mathcal{P} \leftarrow \text{HEATMAP\_ESTIMATION}(M, \delta, F)$ 
6:    $M, \mathcal{P} \leftarrow \text{COARSE\_REDUCTION}(M, \delta, F, \mathcal{P})$ 
7:    $M \leftarrow \text{FINE\_REDUCTION}(M, \delta, F, \mathcal{P})$ 
8:
9:   // Attack (Perturbation Boosting)
10:   $A, \delta \leftarrow \text{BOOST}(x, \delta, M, F, y_{tar})$ 
11: end for

```

---

ter chooses a pre-selected patch location. Our white-box GRAPHITE algorithm also finds successful transform-robust attacks for a much higher set of victim-target pairs than the Patch-PGD attack. Finally, our white-box algorithm does not require a user to specify the shape or size of the mask or its location. Example images of these attacks are included in Fig. 2.

## 5. Black-box (Hard-label) Automatic Physical Attacks

We now seek to instantiate our GRAPHITE framework to solve the automatic physical attack formulation from (1) in the black-box hard-label setting. Our white-box algorithm (Section 4.1) cannot be trivially extended to a black-box setting, as selecting relevant pixels for removal is not easily achieved without gradient access.

We also note that prior hard-label attack work [20] suggests that gradient estimation in high-dimensional settings is noisy and difficult to optimize, so we explore settings where perturbations are generated in smaller resolutions and then optionally resized to apply to larger resolution victim images.

This section is organized as follows: we begin by again leveraging the C&W  $\ell_0$  algorithm, now in combination with existing digital black-box attacks, to present three “baseline” black-box instantiations of GRAPHITE. We leverage insights from the insufficiencies of these baselines to (a) present a novel algorithm for the pixel selection and removal procedures (lines 4 and 5 of Algorithm 1), referred to as “mask generation”, and (b) adopt Randomized Gradient Free (RGF) optimization of transform-robustness itself as the attack procedure (line 6 of Algorithm 1), referred to as “perturbation boosting”.

### 5.1. Baselines

As discussed above, all baselines adopt the C&W pixel selection and removal strategies, as in our white-box instantiation. Instead, each baseline differs only in terms of choice of inner attack (line 6 of Algorithm 1). For our first two baselines, we adopt a vanilla and EoT version of the digital black-box OPT-attack [20]. OPT-attack is a suitable replacement for the EoT PGD attack employed in our white-box algorithm, as it is able to craft attacks in the black-box setting, and provide estimated gradients that can be used to order pixels for pixel selection and removal. For our third baseline, we deviate from OPT-attack and instead adopt perturbation boosting — our RGF optimization attack that leverages transform-robustness itself as the objective function. We provide details for each baseline below, followed by experimental results.

**5.1.1.  $\ell_0$  and OPT baseline.** This baseline employs the vanilla OPT-attack [20] as its choice of attack algorithm. OPT-attack crafts an adversarial example using a distance based objective:

$$\operatorname{argmin}_{\theta} g(\theta) \quad (2)$$

where the objective  $g(\theta)$  is the distance to the decision boundary, formally defined as:

$$\operatorname{argmin}_{\mu > 0} \mu \text{ s.t. } \left( F \left( x + \mu \frac{\theta}{\|\theta\|_2} \right) = y_{tar} \right) \quad (3)$$

and where  $\theta$  is the direction and  $\mu$  is the distance to the nearest adversarial example  $x^*$  in that direction.

This attack is suitable for GRAPHITE— it returns both an adversarial example, and estimated gradients for (2) which can be used for pixel selection/removal. We consider an attack a success so long as it elicits misclassification, regardless of transform-robustness (as transforms have not been incorporated in any manner).

**Results.** To evaluate this baseline, we run targeted attacks for all 90 victim-target pairs in the 10 class subset of GTSRB used in Section 4.1. All hyper-parameters are identical to those used in our white-box experiments, and performed on 32x32 images. Results are presented in the first row of Table 2, and a sample is presented in the first column of Table 3. It is clear that OPT-attack, while able to find successful attacks (as per our definition above), results in examples that are of extremely low transform-robustness  $\sim 1.5\%$ . This is likely an artifact of (2) not incorporating transforms in any manner. OPT-attack also results in a significant number of queries ( $\sim 920k$ ), as a result of its intense decision boundary-searching procedures. The final mask size is the only aspect of this

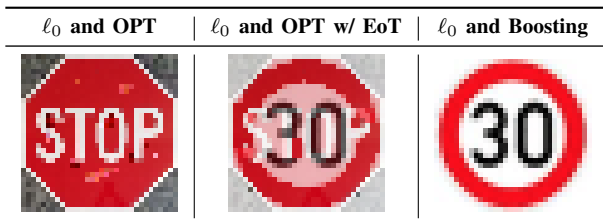
TABLE 1. WHITE-BOX COMPARISONS BETWEEN OUR WHITE-BOX VERSION OF GRAPHITE (ALGORITHM 3) AND A PATCH-PGD ATTACK THAT TRIES THE 4 CORNERS AND THE CENTER ON 90 VICTIM-TARGET TRAFFIC SIGN PAIRS. WHILE PATCH-PGD CAN PERFORM WELL ON THE RIGHT EXAMPLES, GRAPHITE CAN MUCH MORE RELIABLY AND QUICKLY FIND SUCCESSFUL ATTACKS WITH LESS PERTURBATION SIZE. TR STANDS FOR TRANSFORM-ROBUSTNESS.

Method	Avg. TR, All	Avg. Mask Size, All	Num. >80% TR	Avg. TR, >80% Samples	Avg. Mask Size, >80% Samples	Avg. Inferences
GRAPHITE	77.53%	8.82%	84	80.60%	6.35%	40,475.6
Patch-PGD	10.1556%	6.88%	4	95.25%	6.88%	100,000

TABLE 2. QUANTITATIVE RESULTS FOR HARD-LABEL BASELINE ATTACKS. WE REPORT THE AVERAGE AND STANDARD DEVIATION OF TRANSFORM-ROBUSTNESS, # OF PIXELS OUT OF  $32 \times 32 = 1024$  IN THE MASK (I.E.,  $\ell_0$  DISTANCE), AND NUMBER OF QUERIES ISSUED TO THE MODEL. STATISTICS ARE PRESENTED ONLY FOR SUCCESSFUL ATTACKS (I.E., ATTACKS THAT ARE ABLE TO CRAFT AN ADVERSARIAL EXAMPLE).

Baseline	# Successes	Transform-robustness (%)	Queries	Mask Size
$\ell_0$ and OPT	90/90	$1.52 \pm 4.26$	$919.82k \pm 605.24k$	$244.36 \pm 307.11$
$\ell_0$ and OPT with EoT	81/90	$80.01 \pm 0.11$	$1958.67k \pm 1317.49k$	$601.90 \pm 190.91$
$\ell_0$ and Boosting	81/90	$97.89 \pm 3.61$	$5.50k \pm 9.17k$	$990.72 \pm 56.78$

TABLE 3. SAMPLES FROM OUR THREE HARD-LABEL BASELINE ATTACKS. SHOWN ARE TARGETED ATTACKS FROM A STOP SIGN TO SPEED LIMIT 30 KM / HR SIGN. THE LEFTMOST IMAGE SUFFERS FROM EXTREMELY LOW TRANSFORM-ROBUSTNESS. THE MIDDLE AND RIGHTMOST IMAGES EXHIBIT HIGHER TRANSFORM-ROBUSTNESS AT THE COST OF EXTREME VISIBLE ARTIFACTS FROM THE TARGET IMAGE.



baseline that is modestly respectable, with a perturbation that covers  $\sim 24\%$  of the input image.

**5.1.2.  $\ell_0$  and OPT with EoT baseline.** This baseline employs an EoT version of OPT-attack [20] as its choice of attack algorithm, in an attempt to alleviate the low transform-robustness of the first baseline. We first define a wrapper function  $W(x)$ :

$$W(x) = \begin{cases} y & \text{if } \mathbb{E}_{t \sim T} \left[ F(t(x)) = y_{tar} \right] \geq 80\% \\ -1 & \text{otherwise} \end{cases} \quad (4)$$

Then, with this wrapper function, we modify  $g(\theta)$  to the following:

$$\operatorname{argmin}_{\mu > 0} \mu \text{ s.t. } \left( W \left( x + \mu \frac{\theta}{\|\theta\|_2} \right) = y_{tar} \right) \quad (5)$$

This attack is again suitable for GRAPHITE, for the same reasons as before. However, we now consider an attack a success only if it exhibits a transform-robustness greater than the  $tr_{min}$  threshold, as this baseline directly incorporates transforms via EoT.

**Results.** To evaluate this baseline, we repeat the experimental setup used for the first baseline. We also initialize the perturbation direction  $\theta$  using the target image. Results are presented in the second row of Table 2, and a sample is presented in the second column of Table 3.

As expected, the introduction of EoT significantly raises average transform-robustness to  $\sim 80\%$ . However, this has come at the cost of doubling in queries  $\sim 1,959k$ , and an unacceptably large mask size covering nearly 59% of the input image. In other words, *wrapping existing hard-label attacks with EoT is an inefficient approach to generating small attacks with high transform-robustness.* Additionally, we observe that even for the successful attacks, OPT attack is unable to escape the initial perturbation direction (i.e., the target image itself). This results in attack examples with very visible artifacts from the target.

**5.1.3.  $\ell_0$  and Boosting Baseline.** This baseline employs perturbation boosting as its choice of attack algorithm, i.e., an RGF optimization attack that leverages transform-robustness itself as the objective function. This choice is motivated by the intuition that directly optimizing for our desired metric (instead of a proxy objective function provided by existing black-box attacks) is likely a more straightforward optimization problem, which is likely to result in fewer queries and a smaller mask, while still achieving high transform-robustness. For further details regarding the details and suitability of perturbation boosting for GRAPHITE, see Section 5.4, where it becomes a part of our final, recommended instantiation algorithm for GRAPHITE in the black-box setting.

**Results.** To evaluate this baseline, we again repeat the experimental setup used for the first baseline. We initialize the perturbation using the target image. Results are presented in the third row of Table 2, and a sample is presented in the third column of Table 3. As expected (since we are now directly maximizing transform-robustness) this baseline observes a near optimal  $\sim 98\%$  transform-robustness, with significantly less queries than previous baselines ( $\sim 5.5k$ ). Unfortunately, this baseline still continues to suffer from unacceptably large masks covering nearly 97% of the input image. Close inspection reveals that this is because the estimated RGF optimization gradients eventually become zero at some iteration (i.e., the area around the example appears to be flat, thereby obstructing sampling-based based techniques like RGF). Zero gradients prevent the algorithm from creating a reliable importance ordering of pixels, thereby ending

the attack as pixel selection/removal cannot proceed. This also results in several artifacts from the target image, as 1-2 rounds are not enough to create a sufficiently small mask, or produce a more obscure perturbation.

## 5.2. Two-Step Optimization

Our black-box baseline instantiations in Section 5.1 failed to craft acceptable automatic physical attacks. However, these failures provided key insights towards satisfying our three core requirements for automatic physical attacks: (a) creating high transform-robustness examples requires direction incorporation of transforms (EoT) into the attack, (b) naïve application of EoT to existing black-box attacks is an indirect and query-inefficient approach to doing so, and (c) reliance upon a gradient-based pixel ordering can fail in the black-box setting, thus leading to large masks.

As a result, we instead solve a *decoupled optimization problem* that first generates a suitable mask and then boosts the transform-robustness of the perturbation given such a mask. This decoupled problem can be viewed as heuristically solving the general framework presented in Algorithm 1 with a single iteration, with mask generation taking care of pixel selection and removal and perturbation boosting becoming the internal attack. This solution then forms the basis for our primary, recommended hard-label instantiation of GRAPHITE, as shown in Algorithm 4.

**Step #1: Mask Generation:** We first find an optimized mask that, when filled in with the target image  $x_{tar}$ , results in at least a specified level of transform-robustness,  $tr_{lo}$ , a hyperparameter. We constrain the unmasked perturbation to be fixed at  $\delta_{tar} = x_{tar} - x$  and solve the optimization objective from (1) under that constraint:

$$\begin{aligned} \operatorname{argmin}_M \lambda \cdot \|M\|_0 - \mathbb{E}_{t \sim T} \left[ F \left( t(x + M \cdot \delta_{tar}) \right) = y_{tar} \right] \\ \text{s.t. } \mathbb{E}_{t \sim T} \left[ F \left( t(x + M \cdot \delta_{tar}) \right) = y_{tar} \right] \geq s_{lo} \end{aligned} \quad (6)$$

We show how to solve this formulation heuristically using an algorithm described in Section 5.3. Note that  $\delta_{tar}$  is only applicable within the resulting mask  $M$ .

**Step #2: Perturbation Boosting:** Equipped with the mask  $M$  found by the Mask Generation Optimization Problem in Step #1, we then aim to maximize transform-robustness for the given mask by changing the perturbation  $\delta$  within the masked region:

$$\operatorname{argmax}_{\delta} \mathbb{E}_{t \sim T} \left[ F \left( t(x + M \cdot \delta) \right) = y_{tar} \right] \quad (7)$$

By using transform-robustness as a measure of physical robustness, we can leverage this function as an optimization goal we can pursue even in the hard-label case (described in Section 5.4). In Section 5.5, we provide empirical evidence that this reformulation based on transform-robustness is approximately continuous. We do this by showing that the objective has relatively low Lipschitz constants even when approximating the expectation in (7) by averaging over  $n$  transformations. We additionally refer to this process as *boosting* the transform-robustness, as it aims to make transform-robustness as high as possible.

## 5.3. Mask Generation Algorithm

For the first step of our hard-label GRAPHITE instantiation, we need to find a candidate mask that has good initial transform-robustness and small size. Boosting can take care of further improving the transform-robustness as long as it samples enough variance at nearby points to make useful gradient estimates with RGF. We first set the perturbation to the target image’s pixels within the mask. In other words, the initial attack is  $x + M \cdot (x_{tar} - x)$ .

We generate masks using a three stage process:

- 1) Heatmap Estimation
- 2) Coarse-grained Mask Reduction
- 3) Fine-grained Mask Reduction

We first initialize the mask to the entire victim object, which overlays the target object over the victim. We then choose a group of pixels called a *patch* as a configurable input into the algorithm. We then collect all patches of a given shape (e.g.  $4 \times 4$  squares) that overlap with the victim object. These patches serve two purposes: (1) it helps us estimate a “heatmap” (i.e., which regions of pixels contribute more to transform-robustness) and (2) it is used to remove groups of pixels from the mask to reduce its size as the algorithm optimizes the mask objective function (6). The shape size such as  $4 \times 4$  square (rather than a single pixel) helps ensure that the attack image is not too pixelated and thus more likely to be implementable as a physical perturbation such as via stickers.

This process can be visualized by imagining a thin overlay of the target being placed on top of the victim, and then slowly cutting regions out of the overlay, exposing the victim object underneath.

**5.3.1. Heatmap Estimation.** We generate a “heatmap” (similar to a saliency map) over the victim image to begin the process of pixel selection and removal. This could be any process that generates an ordering of pixel patches. We mainly focus on one strategy that we call a “target-based heatmap” strategy, which orders patches relative to transform-robustness drops with respect to the target.

Specifically, for each patch  $p$  that overlaps with the victim object, we measure the transform-robustness of the mask  $M$  and perturbation  $\delta_{tar}$ , where  $M$  includes every pixel of the victim object except for  $p$ . In other words, we take the original target image overlay, cut out  $p$ , and measure the resulting transform-robustness. If the transform-robustness drops a lot after removing  $p$ , those target pixels are important to causing a target prediction. This enables us to identify candidate regions to remove from the mask. We refer to this drop in transform-robustness as the *impact* of that patch and output the sorted list of patches in increasing impact.

The size of the patches matters in the hard-label setting. If we pick just a single pixel as our patch, the transform-robustness would likely be the same with or without it, making the heatmap useless. If we make the patch too large, we lose the ability to make more general mask shapes. For  $32 \times 32$  noise, we empirically found that a  $4 \times 4$  square patch worked well.

We note that the “target-based heatmap” approach can successfully evaluate patches with varying degrees of transform-robustness drops, leading to a useful ordering.

One could imagine a “victim-based heatmap” where we try adding small sections of the target onto the victim, but we found that this approach just led to calculating  $\approx 0\%$  transform-robustness for almost all patches. We experiment with a random heatmap strategy in Section 6.3.

**5.3.2. Coarse-grained Mask Reduction.** Using the sorted list of patches from heatmap estimation, we begin reducing the size of the mask. As an optimization to save queries, we first do a coarse-grained reduction that binary searches for a pivot in the patch list. We find the point *pivot* in the ordered list of patches  $\mathcal{P}$  such that the bitwise unions of patches from that point ( $\bigcup_{i=pivot}^{|\mathcal{P}|} \mathcal{P}_i$ ) yields a mask of transform-robustness  $\geq tr_{hi}$ , where  $tr_{hi}$  is a hyper-parameter specifying a high transform-robustness threshold that must be reached. If  $tr_{hi}$  cannot be reached, we simply include all patches. Coarse-grained reduction outputs  $L_c$ , the list of patches from *pivot* to the end.

**5.3.3. Fine-grained Mask Reduction.** We then execute a fine-grained reduction that uses a greedy algorithm to improve the objective function of (6). Fine-grained reduction takes  $L_c$  and evaluates each patch in sorted order. It removes the patch if its removal improves the objective function and keeps it otherwise. Empirically, we found that it was important to add the restriction that transform-robustness does not cross below some minimum threshold,  $tr_{lo}$  to ensure success in boosting. The end result is the final mask defined by the union of the retained elements of  $L_c$ . Because the objective function rewards small masks and high transform-robustness, the final mask balances both well.

We can optionally specify to GRAPHITE that we desire a maximum mask size  $m_{max}$ . If this option is activated, we can simply break early once we drop below  $m_{max}$ . If the first iteration fails to get below  $m_{max}$ , then the value of  $\lambda$  (the weight of the mask size term in the joint optimization problem in (1)) can be increased until an iteration gets below  $m_{max}$ .

Let  $n$  be the number of transforms used for estimating transform-robustness. Heatmap estimation uses  $n \cdot |\mathcal{P}|$  queries, coarse-grained reduction uses  $n \cdot \log |\mathcal{P}|$  queries, and fine-grained reduction uses  $n \cdot |L_c|$  queries.

## 5.4. Perturbation Boosting Algorithm

Given a resulting image  $x$  and a mask  $M$  from the previous stage, transform-robustness boosting, or simply *boosting*, aims to find the perturbation  $\delta$  that maximizes transform-robustness. We propose a *transform-robustness-based* reformulation to use with RGF [32], [33] to find the perturbation within the mask  $M$  with maximum transform-robustness, which works as follows.

The perturbation  $\delta$  is first initialized to  $M \cdot (x_{tar} - x)$  and then we proceed to maximize the probability that a perturbation remains robust to physical-world transforms with the RGF [32], [33] method for gradient estimation using  $q$  random samples for each gradient estimation. Explicitly, let  $u$  be random Gaussian unit vectors within the allowable range of the mask and let  $\beta$  be a nonzero smoothing parameter. Then, we set  $\delta$  to  $\delta - \eta \cdot \hat{g}$  where  $\eta$  is the step size and  $\hat{g}$  is the gradient, calculated as follows:

$$\hat{g} = \frac{TR(M, \delta + \beta u) - TR(M, \delta)}{\beta} \cdot u \quad (8)$$

where  $TR(M, \delta)$  refers to the estimated transform-robustness for a mask  $M$  and a perturbation  $\delta$ .

Finally, we introduce the notion of a query budget which limits the amount of queries used in a particular stage of the algorithm. These parameters can be tuned to emphasize better mask generation or better boosting without a budget of queries if we want to limit the number of attack queries.

## 5.5. Suitability of Transform-Robustness Reformulation

To demonstrate that our reformulation based on transform-robustness is approximately continuous for successful RGF optimization, we show empirically that our objective has a low local Lipschitz constant. We execute boosting on attack examples from Stop sign to Speed Limit 30 km/hr, Stop sign to Pedestrians, and Stop sign to Turn Left Ahead with  $n = 1000$  transformations and approximate the local Lipschitz constant every time we compute  $TR(M, \delta + \beta \cdot u)$ . The approximate local Lipschitz constant is given by  $\frac{|TR(M, \delta + \beta \cdot u) - TR(M, \delta)|}{|\beta \cdot u|}$ . We found that the maximum observed local Lipschitz constant was 0.056. We include a histogram of observed local Lipschitz constants in Fig. 3.

## 6. Experiments

In this section, we demonstrate the viability of our black-box GRAPHITE instantiation presented in Algorithm 4 and Sections 5.2–5.4, henceforth referred to as simply GRAPHITE unless otherwise specified. Specifically, we evaluate GRAPHITE by attacking a traffic sign classifier trained on GTSRB [40] data. We first report transform-robustness results on all 1,806 possible victim target pairs in GTSRB. Then, we print stickers on a smaller subset of attacks, and conduct real-world field tests to show that our results carry over to the real-world. We analyze 420 field test images over two victim-target pairs of signs under a variety of viewpoint and lighting conditions. We also conduct a drive-by test similar to Eykholt et al. [18]. Finally, we explore our pipeline’s ability to adapt to attacker priorities/constraints, allowing for a trade-off between transform-robustness, mask size, and query budget.

### 6.1. Experimental Setup

This section discusses our experimental setup for running GRAPHITE.

**Datasets and Classifiers.** We use the classifier from RP<sub>2</sub> [18], [41] trained on an augmented GTSRB dataset [40]. As with RP<sub>2</sub> [18], we replace the German Stop signs with U.S. Stop signs from the LISA dataset [42]. As a validation set, we take out the last 10% from each class in the training set. We augment the dataset with random rotation, translation, and shear, following Eykholt et al. [18]. Our network, GTSRB-Net, has a 97.656% test set accuracy.

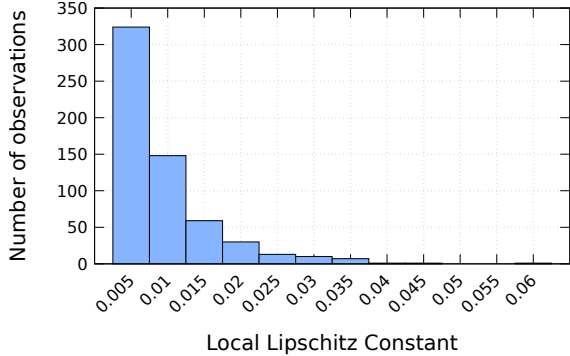


Figure 3. A histogram of our approximate local Lipschitz constant observations on transform-robustness. This graph shows that transform-robustness does not vary too much per amount of change with a sufficient number of transformations.

As in our white-box experiments in Section 4.1, we use Internet images outside of the dataset plus our own Stop sign picture since we had a physical sign available for initialization to demonstrate that GRAPHITE does not rely on having training set images to initialize from. In our experiments we assume that object boundaries are available, but note they could be obtained automatically through an object segmentation network [43].

**GTSRB Attack Details.** We set the size of our input images to be  $244 \times 244$ . During the attack, we generate  $32 \times 32$  perturbations and then upsample the perturbations to the resolution of the input image when they are added. Reducing the dimensionality of the perturbation space makes RGF more efficient [20] and can help encourage blockier perturbations that can be sensed by a camera in the physical-world.

For field testing, we print stickers and place them on a  $30'' \times 30''$  Stop sign and place it at stationary positions to test how robust our attacks are to different viewing conditions. We take five pictures of the perturbed Stop sign at 14 different locations for a total of 70 pictures per set. To test lighting conditions, we take one set of images in outdoor light and two sets indoors, one with indoor lights on and one without. To compare against baseline Stop sign accuracy, we also take five pictures of a clean Stop sign at each of the same 14 locations. The 14 locations were chosen based on  $RP_2$  evaluation [18].

To gather crops we use the original author’s YOLOv3 [44] object detector network trained on MS COCO [45] to predict bounding boxes for the Stop sign. We take the output bounding boxes, crop the sign, resize to  $32 \times 32$ , and feed through our network for classification. Further hyperparameters are specified in Table 4.

## 6.2. Experimental Results

**Digital Transform-Robustness Results.** We report results for all 1,806 possible GTSRB victim target pairs in Table 5. On average, we observe masks with an  $\ell_0$  distance of 170.3 (16.6% w.r.t. the  $32 \times 32$  image area) and 77.8% transform-robustness.

In Table 6 we provide results from attacks between all victim target pairs of a subset of 10 varied GTSRB

TABLE 4. HYPERPARAMETERS FOR BLACK-BOX GRAPHITE EXPERIMENTS. ALL RANGED PARAMETERS SAMPLED UNIFORMLY.

Parameter	Value
RGF smoothing parameter ( $\beta$ )	1
RGF step size ( $\eta$ )	500
Boosting query budget ( $b$ )	20k
# Samples for RGF gradient sampling ( $q$ )	10
Rotation range about the $y$ axis	$(-50^\circ, 50^\circ)$
Base focal length ( $f$ )	3 ft.
Crop sizes and offsets	$(-3.125\%, 3.125\%)$
Lighting gamma value ( $\gamma$ )	(1, 3.5) and (1, 1/3.5)
Gaussian kernels for blurring	[1, 3, 5, 7]
Joint optimization mask size weight ( $\lambda$ )	5
# of transforms ( $n$ )	100
Transform-robustness high threshold for coarse red. ( $tr_{hi}$ )	85%
Transform-robustness low threshold for fine red. ( $tr_{lo}$ )	65%
Max mask size option ( $m_{max}$ )	Not set

TABLE 5. QUANTITATIVE RESULTS OF DIGITAL GTSRB ATTACKS. AVERAGE AND STANDARD DEVIATION OF TRANSFORM-ROBUSTNESS, # OF PIXELS OUT OF  $32 \times 32 = 1024$  IN THE MASK (I.E.,  $\ell_0$  DISTANCE), NUMBER OF QUERIES REPORTED FOR THE GIVEN VICTIM TO ALL OTHER TARGETS.

Victim	Stop	SL 30 km/hr	Avg. of all 43 victims
Surv. (%)	$80.8 \pm 7.02$	$84.5 \pm 10.6$	$77.8 \pm 17.5$
Mask Size	$116 \pm 38.0$	$139 \pm 71.7$	$170.3 \pm 122$
# Queries	$133k \pm 8.92k$	$134k \pm 15.2k$	$126k \pm 18.9k$

signs. We include the final output image, the transform-robustness, and the mask size. GRAPHITE generally finds small, highly transform-robust perturbations on a variety of attacks. The examples that tend to not perform as well are attacks on a triangle sign victim, as overcoming the difference in shape is difficult. Furthermore, it is not a large enough space to fit the entire target object on the victim. This means that in reduction the starting transform-robustness may be low to begin with, making it hard to prune patches from the mask. Resizing the target image to fit within the victim image may alleviate this concern. In general, we find the attack quality varies depending on the victim target pair, which is consistent with prior work that finds the distortion to vary drastically depending on the attack pair [14].

**Physical Transform-Robustness Field Tests.** We also conduct field experiments to confirm that our results carry over to the physical world. We evaluate GRAPHITE on a targeted Stop sign attacks to targets of Speed Limit 30 km/hr and Pedestrians at different viewing angles and lighting.

Table 7 shows the results of the field tests for GTSRB. On average, they took 131k queries. The Speed Limit 30 km/hr attack was successful over all three lighting conditions with at least 92.9% physical robustness. The Pedestrians attack also did well, with at least 85.7% success rate over each lighting condition. Overall, these results suggest that transform-robustness translates reasonably well into the physical world and improvements in transformations could further improve the translation. Baseline Stop sign tests were at least 95.7% in each lighting condition.

TABLE 6. SAMPLE OF DIGITAL TARGETED ATTACKS ON GTSRB-NET. RAN WITH  $s_{lo} = 65\%$ ,  $s_{hi} = 85\%$ ,  $n = 100$  TRANSFORMS. FOR CELLS WITH SAME VICTIM AND TARGET, WE REPORT THE % OF TRANSFORMS THE ORIGINAL LABEL IS PREDICTED. MASKS SIZE IS REPORTED IN TERMS OF # OF PIXELS IN  $32 \times 32$  (I.E.,  $L_0$  IN  $32 \times 32$  SPACE).

Victim	Target									
Transform-robustness	92%	86%	85%	79%	80%	82%	80%	90%	77%	71%
Mask Size	0	88	123	105	51	96	131	92	138	97
Transform-robustness	77%	100%	88%	94%	94%	89%	88%	99%	61%	93%
Mask Size	161	0	18	140	74	152	175	45	210	156
Transform-robustness	79%	97%	88%	87%	88%	91%	95%	97%	62%	65%
Mask Size	171	13	0	228	132	173	162	41	213	122
Transform-robustness	50%	73%	52%	95%	86%	79%	100%	0%	79%	88%
Mask Size	398	398	398	0	198	254	28	398	205	190
Transform-robustness	73%	85%	71%	85%	100%	81%	71%	80%	71%	71%
Mask Size	111	72	120	92	0	122	93	74	263	148
Transform robustness	0%	58%	7%	4%	92%	100%	46%	87%	83%	57%
Mask Size	436	436	436	436	81	0	436	157	198	436
Transform robustness	56%	84%	70%	90%	80%	69%	100%	0%	78%	77%
Mask Size	398	398	398	23	133	225	0	398	133	161
Transform-robustness	74%	91%	73%	86%	77%	78%	76%	99%	72%	69%
Mask Size	172	43	75	92	62	106	133	0	218	114
Transform-robustness	72%	83%	82%	74%	91%	92%	78%	90%	73%	79%
Mask Size	142	123	141	159	137	137	175	90	0	182
Transform-robustness	79%	89%	89%	81%	82%	67%	82%	91%	73%	99%
Mask Size	42	85	79	106	106	153	117	62	242	0

**Physical GTSRB Drive-by Tests.** In this section, we provide extended field test results for GTSRB under additional imaging conditions, in the form of drive-by tests. In particular, we record videos while driving towards the sign in a private lot, simulating a realistic driving environment in an allowable fashion<sup>1</sup>. We test each of the two attacks from Table 7. As in prior work by Eykholt et al. [18], we analyze every 10th frame from the video. We use the same YOLOv3 [44] detector as the other GTSRB results to crop our frames. Some frames, particularly ones at the beginning of the video when we were farthest

away could not be cropped with YOLOv3 and were thus cropped manually in a similar fashion.

We include results for these two stop sign attacks in Table 8. The Speed Limit 30 km/hr attack was the most successful, with 97.5% physical robustness, which is inline with the field test results in Table 7 and above the digital transform-robustness. The Pedestrians attack was also successful with an 82.1% physical robustness rate, which is right around the its transform-robustness of 79%.

Overall, these results confirm the field test results reported in Table 7 in an even more realistic driving setting. Example images are included in Appendix C.

1. We follow local laws and regulations for safety in this test.

TABLE 7. GTSRB FIELD TEST RESULTS. PHYSICAL ROBUSTNESS RESULTS ARE CALCULATED OVER 5 PICTURES EACH AT THE FOLLOWING SPOTS: 5 FT  $\times$  {0°, 15°, 30°, 45°}, 10 FT  $\times$  {0°, 15°, 30°}, 15 FT  $\times$  {0°, 15°}, 20 FT  $\times$  {0°, 15°}, 25 FT, 30 FT, 40 FT. EACH EXAMPLE WAS TESTED 3 TIMES: OUTDOORS, INDOORS WITH INDOOR LIGHTS TURNED OFF, AND INDOORS WITH INDOOR LIGHTS TURNED ON.

Victim	Target	Digital GRAPHITE attack	Physical GRAPHITE attack (outdoors)	Dig. Surv. (100 xforms)	Phys. Surv. (Indoors, lights off)	Phys. Surv. (Indoors, lights on)	Phys. Surv. (Outdoors)
				86%	92.9%	94.3%	100%
				79%	97.1%	85.7%	100%

TABLE 8. EXTENDED GTSRB FIELD TEST RESULTS, INCLUDING THE MEASURED PHYSICAL ROBUSTNESS OF THE VIDEO FRAMES. EVERY 10TH FRAME OF THE VIDEOS WERE ANALYZED.

Target	# Frames Analyzed	Attack Success Rate (Transform-robustness)
Speed Limit 30 km/hr	40	97.5%
Pedestrians	39	82.1%

TABLE 9. COMPARISON OF THE ORIGINAL TARGET-BASED HEATMAP VS. A RANDOM HEATMAP STRATEGY. THE NUMBER OF QUERIES CAN BE DRASTICALLY DECREASED WITH, ON AVERAGE, SOME INCREASE IN MASK SIZE AND SOME DECREASE IN TRANSFORM-ROBUSTNESS. AVERAGE AND STANDARD DEVIATION ARE PRESENTED.

Strategy	Orig. Strategy with Target Heatmap	Random Heatmap	Min Query Setting
Surv. (%)	77.8 $\pm$ 17.5	76.4 $\pm$ 17.1	19.9 $\pm$ 21.2
Mask Size	170.3 $\pm$ 122	175.9 $\pm$ 121	112.993 $\pm$ 69.7
# Queries	126k $\pm$ 18.9k	62.1k $\pm$ 12.5	572 $\pm$ 105

### 6.3. Variations and Tuning of GRAPHITE

We now explore GRAPHITE’s ability to trade-off transform-robustness, mask size, and query count as well as an examination of heatmap estimation strategies. We also examine GRAPHITE’s output without the restriction that the noise be contained within the victim object.

**6.3.1. Reducing the Number of Queries.** To further reduce the number of queries, we consider two adjustments: 1) reducing the number of transforms and 2) replacing the target-based heatmap strategy with a random heatmap strategy that simply orders patches randomly. We also test a “minimum query” setting, which uses both adjustments to the extreme: both the random heatmap and the use of only one transform.

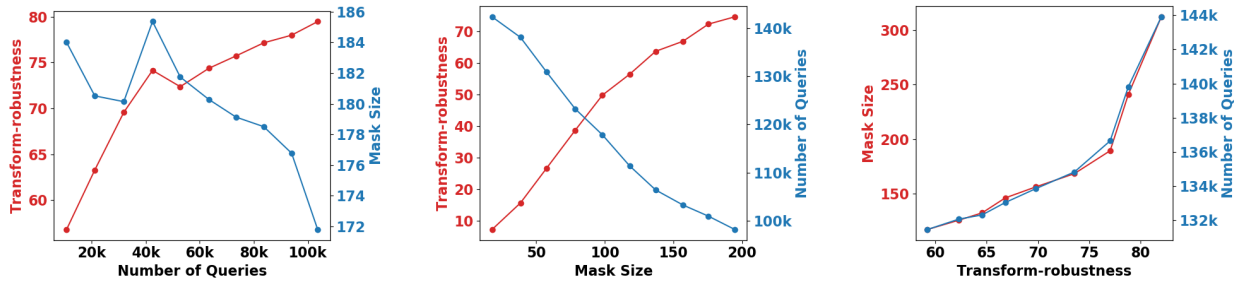
**Tuning the Number of Transformations.** We first begin by decreasing  $n$  (the number of transformations) that we use in mask generation and boosting. This makes every transform-robustness measurement run faster. To ensure the numbers are comparative, we test each setting under the default  $n = 100$  transformation setting.

We test with  $n = 10, 20, 30, 40, 50, 60, 70, 80, 90, 100$  transforms. We test the 90 non-identity victim-target pairs from Table 6. The results of these tests are shown in Fig. 4a. Since the number of queries scales monotonically with the number of transforms, we plot the 10 points using the number of queries on the  $x$  axis, and with the transform-robustness and mask size on the two  $y$  axes. As more transforms are used in the mask generation and boosting processes, the quality of the generated attack increases, i.e., the size of the mask decreases and the transform-robustness of the results increases. Intuitively,

this makes sense - as the number of transformations are increased, the objective becomes smoother and the estimates become more accurate. This performance benefit comes at the trade-off of increased query count and thus, if given a specific query budget, an attacker could tune this parameter based on their query restrictions.

**Random Heatmap.** For this variation, we consider replacing the target-based heatmap estimation process with a random heatmap strategy that simply orders the patches randomly. Because the patches no longer offer any meaningful order, we also remove the coarse-grained reduction process as it involves a binary search over the patch list. This reduces the queries by saving an iteration over patch transform-robustness estimations. While we lose the ability to binary search, we save several thousand queries with this change. The objective function of (6) rejects the removal of extremely bad choice of patches, but can suffer from poor removal choices early on that negatively influence the final result.

The results of this experiment are shown in Table 9, run over all 1,806 victim-target pairs. The random heatmap strategy performs quite similarly to the original target-based heatmap strategy with only about half of the queries, with the average number of queries dropping from 126k to 62.1k. The loss in attack quality is a drop from 77.8% to 76.4% transform-robustness and an increase from 170.3 to 175.9 pixels in terms of mask size. So, random heatmap is a viable strategy when query count is a concern. On average, however, the target-



(a) Effects of tuning the number of transforms, on 90 victim-target pairs. Generally, as the number of queries and transformations are increased, the mask size decreases and the transform-robustness increases.

(b) Effects of tuning the max mask size option. As  $m_{max}$  increases, the transform-robustness increases and the query count decreases.

(c) Effects of tuning  $tr_{lo}$ . Generally, as  $tr_{lo}$  increases, the mask size increases as we reject more mask removals and the query count increases some as fewer overlapping patches are removed early.

Figure 4. Effects of trading off query count, mask size, and transform-robustness in our hard-label GRAPHITE pipeline.

based heatmap still provides optimal results in terms of transform-robustness and mask generation.

**Min Queries Setting.** We now combine both of the previous experiments by running GRAPHITE with the random heatmap and with only one transformation, to see if we can get a result that could possibly cause an accident in just the right conditions with the minimum number of queries possible.

The results are shown in Table 9, run over all victim-target pairs. We find that, on average, GRAPHITE can find attacks with 19.9% transform-robustness using only 572 queries. This includes 1,665 / 1,806 victim-target pairs with greater than 0% transform-robustness. The mask size is also small, with an average of 112.993 pixels (11.0% of the image), with fewer transformations for mask generation to have to optimize for. On just the 1665 non-zero transform-robustness examples, the average mask size was 107.897 pixels (10.5% of the image) and the average query count was 566.253 queries. This suggests that risky examples could be generated in as few as a couple hundred queries, but acquiring more robustness to a variety of transformations requires more queries.

**6.3.2. Reducing the Mask Size.** To reduce the mask size, we enable the  $m_{max}$  option and vary it to the desired maximum mask size. We also change  $s_{lo} = 0$  to ensure that the maximum mask size can be reached, even if it means choosing a mask such that the transform-robustness is 0.

We test with  $m_{max}$  values of 20, 41, 61, 82, 102, 123, 143, 164, 184, and 205, which corresponds to 2%, 4%, ..., 20% of the image area. Since mask size increases monotonically as  $m_{max}$  increases, we plot the actual average mask size on the  $x$  axis. The results of these tests are shown in Fig. 4b. The results show an increase in transform-robustness as the minimum mask size increases (and the area to perturb increases) and a decrease in query count, as the algorithm can exit earlier. If a desired mask size limit is desired, then this option can be used.

**6.3.3. Increasing transform-robustness.** To adjust GRAPHITE based on a desired transform-robustness level, we can tune the value of  $s_{lo}$ . By increasing  $s_{lo}$ , we can achieve higher levels of transform-robustness but potentially at the cost of larger mask size. This is because

TABLE 10. COMPARISON OF THE ORIGINAL VICTIM-OBJECT CONSTRAINED ATTACK AND AN ATTACK WHERE THE PERTURBATION CAN BE PLACED ANYWHERE IN THE IMAGE. AVERAGE AND STANDARD DEVIATION ARE PRESENTED.

Strategy	Orig. Strategy, Restricted to Victim Object	Area Unrestricted
Surv. (%)	77.8±17.5	86.7±8.81
Mask Size	170.3±122	147.1±77.8
# Queries	126k±18.9k	149k±20.6

$s_{lo}$  acts like a floor of acceptable transform-robustness while performing mask generation and guarantees a higher transform-robustness point on boosting. So, on average, a higher  $s_{lo}$  should result in higher transform-robustness.

We test with  $s_{lo}$  values of 0.1, 0.2, 0.3, 0.4, 0.5, 0.6, 0.7, 0.8, and 0.9. We fix  $s_{hi}$  to 1.0 for all values of  $s_{lo}$  so that it can remain constant across the tests. The average observed transform-robustness increased monotonically with  $s_{lo}$ , so we plot the actual transform-robustness on the  $x$  axis. The results of these tests are shown in Fig. 4c. The results show an increase in both mask size and number of queries as transform-robustness increases, as expected.

**6.3.4. GRAPHITE without Restricting to the Victim Object Boundaries.** To examine GRAPHITE’s performance in a setting closer to standard patch attacks, we remove the restriction that the perturbation be contained to the victim object.

The results show that GRAPHITE can perform even better if it is not concerned with fitting it in within the boundary of the victim object. The average transform-robustness increases from 77.8% to 86.7% and the mask size drops from 170.3 pixels ( $\approx 16.6\%$  of the image) to 147.1 pixels ( $\approx 14.4\%$  of the image). With more valid patches to evaluate, the query count raises slightly from 126k to 149k. Thus, if the threat model does not need to remain strictly in victim object, smaller attacks can be found with higher transform-robustness.

## 7. Discussion

We now discuss how GRAPHITE performs against a defense called PatchGuard [29], adversarial training, printing and lighting error, and license plate attacks.

TABLE 11. ALPR FIELD TEST RESULTS. TRANSFORM-ROBUSTNESS RESULTS CALCULATED OVER 5 PICTURES EACH AT: {5 FT, 10 FT, 15 FT, 20 FT}  $\times$  {0°, 15°}. LICENSE PLATES ARE EXPIRED PLATES WE ACQUIRED FOR THE PURPOSE OF TESTING THESE ATTACKS. ALL IMAGES CROPPED TO SHOW THE PLATE AREA IN LARGER DETAIL.

Digital GRAPHITE attack	Physical GRAPHITE attack	Phys. transform-robustness	Avg. Lev. Dist.
		82.5%	3.175
		67.5%	1.175

## 7.1. Countermeasures

To the best of our knowledge, there are no defenses that directly aim to mitigate the effects of physical attacks that are realized through arbitrarily-shaped perturbations. Recent work has, however, attempted to address patch attacks (a similar attack where the perturbation is instead restricted to a single patch) [29], [39]. In this section, we investigate whether such defenses are sufficient to defend against attacks from GRAPHITE. To this end, we select PatchGuard [29], a state-of-the-art provably robust defense against patch attacks.

At a high-level, PatchGuard operates by leveraging a CNN with a “small receptive field”, i.e., a CNN where each feature is only influenced by small regions in the input image. This in turn suggests that patch attack perturbations (which occupy small regions in the input image) influence only a few features, and are thus forced to produce abnormally large “suspicious” feature values to elicit misclassification (which can then be masked out). GRAPHITE, however, generates arbitrarily-shaped perturbations. As such, even if the model has a small receptive fields, many features can be influenced by the spread-out perturbations. Intuitively, this suggests that PatchGuard is largely ineffective at defending against GRAPHITE.

**Results.** We evaluate this intuition by launching several GRAPHITE attacks against PatchGuard. Specifically, we sample several victim-target pairs from the CIFAR-10 dataset, and craft GRAPHITE attacks against the authors’ CIFAR-10 BagNet CNN implementation of the PatchGuard defense. We employ transforms adapted for the  $32 \times 32$  CIFAR-10 image size, and pare down specific transforms so that average transform-robustness of CIFAR-10 images themselves is over 50% (rotation about  $y$  axis is reduced to between  $-10^\circ$  and  $10^\circ$ , and lighting variation is removed). Across 50 randomly sampled victim-target pairs, we are able to obtain an average transform-robustness of 72.5% using 153.4k queries with an average mask size of 168.52 pixels. This includes 17 examples with less than 102 pixels (10% of the image) with 70.9% transform-robustness. This suggests that current state-of-the-art defenses against patch attacks are not effective against GRAPHITE, and that future work is necessary to gain robustness against such attacks.

## 7.2. Adversarial Training

We note that GRAPHITE or the white-box automatic physical attack presented in Section 4 could be used in adversarial training to gain robustness to such attacks. In particular, attacks could be tuned as seen in Section 6.3 or in other ways to be more efficient and the parameterization of the GRAPHITE style pipeline enables the generation of multiple attacks per image. We leave exploration of the viability of such an approach to future work.

## 7.3. Printing and Lighting Error

We noticed a limitation in gamma correction to model sun glare and printing deficiencies, particularly when the color blue is involved. See Appendix D for more details.

## 7.4. ALPR Attack

To demonstrate GRAPHITE’s ability to generalize to a real-world system in a different domain, we attack an Automated License Plate Recognition (ALPR) system. We print license plate border stickers and attack expired license plates in physical field tests. The results are shown in Table 11. Details are included in Appendix E.

## 8. Conclusion

We investigated practical, real-world attacks that satisfy three key requirements: that they are automatic, physical, and only require hard-label access. We proposed GRAPHITE, a general framework for generating such automatic attacks, and demonstrated the first instantiation of this framework for hard-label physical attacks on computer vision networks. With GRAPHITE, an attacker can automatically select small areas to perturb with physically-realizable stickers using only query access to the model. GRAPHITE’s attacks are both automatically-generated (e.g., without requiring specification of mask shapes or their location) and highly query-efficient compared to state-of-the-art in both white-box and black-box hard-label settings. In black-box hard-label settings, GRAPHITE is able to generate attacks that are orders of magnitude more efficient in terms of number of queries to the model than other state-of-the-art black-box hard-label attacks. This work deepens our understanding of strategies for generating practical attacks and can be used to test models against realistic threat models. As future direction for research, we plan to explore the use of GRAPHITE framework in adversarial training to help address an open problem – training models to better defend against robust physical perturbation attacks.

## Acknowledgement

This material is based on work supported by DARPA under agreement number 885000, Air Force Grant FA9550-18-1-0166, the National Science Foundation (NSF) Grants 1646392, CCF-FMitF-1836978, SaTC-Frontiers-1804648 and CCF-1652140, and ARO grant number W911NF-17-1-0405. Earlene Fernandes is supported by the University of Wisconsin-Madison Office of

the Vice Chancellor for Research and Graduate Education with funding from the Wisconsin Alumni Research Foundation. The U.S. Government is authorized to reproduce and distribute reprints for Governmental purposes notwithstanding any copyright notation thereon. Any opinions, findings, and conclusions or recommendations expressed in this material are those of the author(s) and do not necessarily reflect the views of our research sponsors.

## References

- [1] K. He, X. Zhang, S. Ren, and J. Sun, "Deep residual learning for image recognition," in *Proceedings of the IEEE conference on computer vision and pattern recognition*, 2016, pp. 770–778.
- [2] A. Krizhevsky, I. Sutskever, and G. E. Hinton, "Imagenet classification with deep convolutional neural networks," in *Advances in neural information processing systems*, 2012, pp. 1097–1105.
- [3] F. Schroff, D. Kalenichenko, and J. Philbin, "Facenet: A unified embedding for face recognition and clustering," in *Proceedings of the IEEE conference on computer vision and pattern recognition*, 2015, pp. 815–823.
- [4] K. Simonyan and A. Zisserman, "Very deep convolutional networks for large-scale image recognition," *arXiv preprint arXiv:1409.1556*, 2014.
- [5] C. Szegedy, V. Vanhoucke, S. Ioffe, J. Shlens, and Z. Wojna, "Rethinking the inception architecture for computer vision," in *Proceedings of the IEEE conference on computer vision and pattern recognition*, 2016, pp. 2818–2826.
- [6] A. Geiger, P. Lenz, and R. Urtasun, "Are we ready for autonomous driving? the kitti vision benchmark suite," in *Computer Vision and Pattern Recognition (CVPR), 2012 IEEE Conference on*. IEEE, 2012, pp. 3354–3361.
- [7] T. P. Lillicrap, J. J. Hunt, A. Pritzel, N. Heess, T. Erez, Y. Tassa, D. Silver, and D. Wierstra, "Continuous control with deep reinforcement learning," *arXiv preprint arXiv:1509.02971*, 2015.
- [8] OpenPilot, "OpenPilot on the Comma Two," <https://github.com/commaai/openpilot>, 2020.
- [9] H. Bou-Ammar, H. Voos, and W. Ertel, "Controller design for quadrotor uavs using reinforcement learning," in *Control Applications (CCA), 2010 IEEE International Conference on*. IEEE, 2010, pp. 2130–2135.
- [10] C. Mostegel, M. Rumpler, F. Fraundorfer, and H. Bischof, "Uav-based autonomous image acquisition with multi-view stereo quality assurance by confidence prediction," in *Proceedings of the IEEE Conference on Computer Vision and Pattern Recognition Workshops*, 2016, pp. 1–10.
- [11] F. Zhang, J. Leitner, M. Milford, B. Upcroft, and P. Corke, "Towards vision-based deep reinforcement learning for robotic motion control," *arXiv preprint arXiv:1511.03791*, 2015.
- [12] N. Carlini and D. Wagner, "Towards evaluating the robustness of neural networks," in *2017 IEEE Symposium on Security and Privacy (SP)*. IEEE, 2017, pp. 39–57.
- [13] I. J. Goodfellow, J. Shlens, and C. Szegedy, "Explaining and harnessing adversarial examples," *arXiv preprint arXiv:1412.6572*, 2014.
- [14] N. Papernot, P. McDaniel, S. Jha, M. Fredrikson, Z. B. Celik, and A. Swami, "The limitations of deep learning in adversarial settings," in *2016 IEEE European symposium on security and privacy (EuroS&P)*. IEEE, 2016, pp. 372–387.
- [15] C. Szegedy, W. Zaremba, I. Sutskever, J. Bruna, D. Erhan, I. Goodfellow, and R. Fergus, "Intriguing properties of neural networks," *arXiv preprint arXiv:1312.6199*, 2013.
- [16] A. Athalye, L. Engstrom, A. Ilyas, and K. Kwok, "Synthesizing robust adversarial examples," *arXiv preprint arXiv:1707.07397*, 2017.
- [17] T. B. Brown, D. Mané, A. Roy, M. Abadi, and J. Gilmer, "Adversarial patch," *arXiv preprint arXiv:1712.09665*, 2017.
- [18] K. Eykholt, I. Evtimov, E. Fernandes, B. Li, A. Rahmati, C. Xiao, A. Prakash, T. Kohno, and D. Song, "Robust physical-world attacks on deep learning visual classification," in *Computer Vision and Pattern Recognition (CVPR)*, June 2018.
- [19] M. Sharif, S. Bhagavatula, L. Bauer, and M. K. Reiter, "Accessorize to a crime: Real and stealthy attacks on state-of-the-art face recognition," in *Proceedings of the 2016 ACM SIGSAC Conference on Computer and Communications Security*, ser. CCS '16, 2016, p. 1528–1540.
- [20] M. Cheng, T. Le, P.-Y. Chen, J. Yi, H. Zhang, and C.-J. Hsieh, "Query-efficient hard-label black-box attack: An optimization-based approach," in *International Conference on Learning Representations*, 2019.
- [21] W. Brendel, J. Rauber, and M. Bethge, "Decision-based adversarial attacks: Reliable attacks against black-box machine learning models," *arXiv preprint arXiv:1712.04248*, 2017.
- [22] T. K. S. Lab, "Experimental security analysis of Tesla AutoPilot," [https://keenlab.tencent.com/en/whitepapers/Experimental\\_Security\\_Research\\_of\\_Tesla\\_Autopilot.pdf](https://keenlab.tencent.com/en/whitepapers/Experimental_Security_Research_of_Tesla_Autopilot.pdf).
- [23] M. Lee and Z. Kolter, "On physical adversarial patches for object detection," *arXiv preprint arXiv:1906.11897*, 2019.
- [24] X. Liu, H. Yang, Z. Liu, L. Song, H. Li, and Y. Chen, "Dpatch: An adversarial patch attack on object detectors," *arXiv preprint arXiv:1806.02299*, 2018.
- [25] A. Fawzi and P. Frossard, "Measuring the effect of nuisance variables on classifiers," in *British Machine Vision Conference (BMVC)*, no. CONF, 2016.
- [26] C. Yang, A. Kortylewski, C. Xie, Y. Cao, and A. Yuille, "Patchattack: A black-box texture-based attack with reinforcement learning," in *European Conference on Computer Vision*. Springer, 2020, pp. 681–698.
- [27] M. Cheng, S. Singh, P.-Y. Chen, S. Liu, and C.-J. Hsieh, "Signopt: A query-efficient hard-label adversarial attack," *arXiv preprint arXiv:1909.10773*, 2019.
- [28] J. Chen, M. I. Jordan, and M. J. Wainwright, "Hopskipjumpattack: A query-efficient decision-based attack," *arXiv preprint arXiv:1904.02144*, 2019.
- [29] C. Xiang, A. N. Bhagoji, V. Schwag, and P. Mittal, "PatchGuard: A Provably Robust Defense against Adversarial Patches via Small Receptive Fields and Masking," in *USENIX Security Symposium*, 2021.
- [30] A. Kurakin, I. Goodfellow, and S. Bengio, "Adversarial examples in the physical world," *arXiv preprint arXiv:1607.02533*, 2016.
- [31] A. Ilyas, L. Engstrom, A. Athalye, and J. Lin, "Black-box adversarial attacks with limited queries and information," in *Proceedings of the 35th International Conference on Machine Learning*, 2018, pp. 2137–2146.
- [32] S. Ghadimi and G. Lan, "Stochastic first-and zeroth-order methods for nonconvex stochastic programming," *SIAM Journal on Optimization*, vol. 23, no. 4, pp. 2341–2368, 2013.
- [33] Y. Nesterov and V. Spokoiny, "Random gradient-free minimization of convex functions," *Foundations of Computational Mathematics*, vol. 17, no. 2, pp. 527–566, 2017.
- [34] N. Papernot, P. McDaniel, and I. Goodfellow, "Transferability in machine learning: from phenomena to black-box attacks using adversarial samples," *arXiv preprint arXiv:1605.07277*, 2016.
- [35] Y. Liu, X. Chen, C. Liu, and D. Song, "Delving into transferable adversarial examples and black-box attacks," *CoRR*, vol. abs/1611.02770, 2016. [Online]. Available: <http://arxiv.org/abs/1611.02770>
- [36] P.-Y. Chen, H. Zhang, Y. Sharma, J. Yi, and C.-J. Hsieh, "Zoo: Zeroth order optimization based black-box attacks to deep neural networks without training substitute models," in *Proceedings of the 10th ACM Workshop on Artificial Intelligence and Security*. ACM, 2017, pp. 15–26.
- [37] N. Narodytska and S. Kasiviswanathan, "Simple black-box adversarial attacks on deep neural networks," in *2017 IEEE Conference on Computer Vision and Pattern Recognition Workshops (CVPRW)*, July 2017, pp. 1310–1318.

- [38] A. Madry, A. Makelov, L. Schmidt, D. Tsipras, and A. Vladu, "Towards deep learning models resistant to adversarial attacks," *arXiv preprint arXiv:1706.06083*, 2017.
- [39] P.-y. Chiang, R. Ni, A. Abdelkader, C. Zhu, C. Studer, and T. Goldstein, "Certified defenses for adversarial patches," *arXiv preprint arXiv:2003.06693*, 2020.
- [40] J. Stallkamp, M. Schlipsing, J. Salmen, and C. Igel, "Man vs. computer: Benchmarking machine learning algorithms for traffic sign recognition," *Neural networks*, vol. 32, pp. 323–332, 2012.
- [41] V. Yadav, "p2-traffic signs," <https://github.com/vxy10/p2-TrafficSigns>, 2016.
- [42] A. Mogelmoose, M. M. Trivedi, and T. B. Moeslund, "Vision-based traffic sign detection and analysis for intelligent driver assistance systems: Perspectives and survey," *IEEE Transactions on Intelligent Transportation Systems*, vol. 13, no. 4, pp. 1484–1497, 2012.
- [43] O. Ronneberger, P. Fischer, and T. Brox, "U-net: Convolutional networks for biomedical image segmentation," in *International Conference on Medical image computing and computer-assisted intervention*. Springer, 2015, pp. 234–241.
- [44] J. Redmon and A. Farhadi, "Yolov3: An incremental improvement," *arXiv preprint arXiv:1804.02767*, 2018.
- [45] T.-Y. Lin, M. Maire, S. Belongie, J. Hays, P. Perona, D. Ramanan, P. Dollár, and C. L. Zitnick, "Microsoft coco: Common objects in context," in *European conference on computer vision*. Springer, 2014, pp. 740–755.

## Appendix A. NP-Completeness of Mask Generation

We now explore the theoretical properties of mask generation and prove its NP-Completeness. Let an  $n \times n$  square grid be represented as  $G_n$ , which is a graph  $(V_n, E_n)$  ( $V_n$  has vertices  $(i, j)$ , where  $0 \leq i \leq n$  and  $0 \leq j \leq n$  and for each  $(i, j)$ ,  $\{(i, j + 1), (i, j - 1), (i + 1, j), (i - 1, j)\} \cap V_n$  is in the set of edges  $E_n$ ). A *mask*  $M$  is a sub-graph of the grid  $G_n$  that corresponds to a contiguous region of squares. Let  $C(G_n)$  be the set of masks corresponding to the grid  $G_n$ . Let  $\mu : C(G_n) \rightarrow \mathbb{R}^+$  be a *monotonic scoring function* ( $M \subseteq M'$  implies that  $\mu(M) \leq \mu(M')$ ). The mask generation problem can be stated as follows: Given  $r$  and threshold  $t$ , find a mask  $M$  of size  $\leq r$  (the size of the mask is number of squares in it) such that  $\mu(M) \geq t$ . We call this problem  $\text{MASK}_P(n, \mu, r, t)$ .

Simply enumerating masks is not feasible because the number of masks could be exponential. We provide a simple argument. Consider a  $k \times k$  sub-grid of  $G_n$ . Consider columns that are odd numbered (i.e. of the form  $(i, \star)$ , where  $i$  is odd). Now any choice of one square for the even columns gives us a contiguous mask, so there are  $\geq 2^{\frac{k(k+1)}{2}}$  masks. There are  $(n - k)^2$   $k \times k$  sub-grids in  $G_n$ . So a lower bound on masks of size  $k$  is at least  $(n - k)^2 2^{\frac{k(k+1)}{2}}$ . Next we prove that our problem is actually NP-complete.

*The Set Cover.* Given a universe  $\mathcal{U}$  and a family  $\mathcal{S}$  of subsets of  $\mathcal{U}$ , a cover is a subfamily  $\mathcal{C} \subseteq \mathcal{P}(\mathcal{U})$  of sets whose union is  $\mathcal{U}$ . In the set-covering decision problem, the input is a triple  $(\mathcal{U}, \mathcal{S}, k)$  ( $k$  is an integer), and the question is *whether there is a set covering of size  $k$  or less*. In the set covering optimization problem, the input is a pair  $(\mathcal{U}, \mathcal{S})$  and the task is to find a set covering that uses the fewest sets. The set-covering decision problem is known to be NP-complete.

**Theorem 1.** Problem  $\text{MASK}_P$  is NP-complete.

**Proof.** Our reduction is from the decision set-cover problem. Assume we are given an instance of the set-cover problem  $(\mathcal{U}, \mathcal{S}, k)$ . Let  $n = \max(|\mathcal{U}|, |\mathcal{S}|)$ . We create a  $n \times n$  grid  $G_n$ . Let  $C(G_n)$  be the set of masks of  $G_n$ . We construct a scoring function  $\mu$  as follows: Let  $M$  be a mask. Let  $I = \{i | (i, 0) \in M\}$ , and  $\mathcal{S}_I = \{S_j | j \in I \wedge S_j \in \mathcal{S}_I\}$ .  $\mu(M) = 1$  if and only if the following condition holds (otherwise  $\mu(M) = 0$ ):  $|I| \leq k$  and  $\cup_{j \in I} S_j = \mathcal{U}$ . It is easy to see that  $\text{MASK}_P(n, \mu, n^2, 1)$  has a satisfying solution iff the instance of the set cover problem has a solution. This proves that the problem is NP-hard. Given a solution to the problem  $\text{MASK}_P(n, \mu, r, t)$ , it is easy to check that it is a valid solution in polynomial time, so the problem is NP. Therefore,  $\text{MASK}_P(n, \mu, r, t)$  is NP-complete.  $\square$

## Appendix B. Transformation Details

Prior work by Eykholt et al. [18] and Athalye et al. [16] model environmental effects to create physical-world attacks in the white-box setting. These transformations account for varying conditions such as the distance and angle of the camera, lighting conditions, etc. Based on this work, we build a more principled set of transformations using classical computer vision techniques. To this end, we group these effects into 3 main classes of transformations:

- 1) **Geometric transformations:** These transformations refer to shape-based changes including rotation, translation and zoom. For planar objects, all three effects can be captured in a single perspective transformation through a homography matrix. Homography matrices relate two planar views under different perspectives. Geometrically, to convert points from one image plane to another, one can break down the operation into a rotation and translation matrix  $R$ , perspective projection onto a plane (P), and an affine transformation from plane to pixels (A). In the planar case, this boils down to a  $3 \times 3$  homography matrix  $H$ :

$$x_{out} = APRx_{in} = Hx_{in} \quad (9)$$

We use these homographies to simulate rotation around the  $y$  axis and different viewing distances for given ranges of values. Once we pick values for each of the parameters uniformly, we construct the homography matrix to compute the transformation.

After performing the perspective transform, we random crop to the tightest square crop that includes the whole object  $\pm c\%$  of the resultant image size to adjust for cropping errors. We also add random offsets for the crop, given as two more parameters. Then, we resize the square to the original resolution.

- 2) **Radiometric transformations:** These are appearance-based transformations with effects such as lighting-based changes. One technique to perform brightness adjustments is gamma

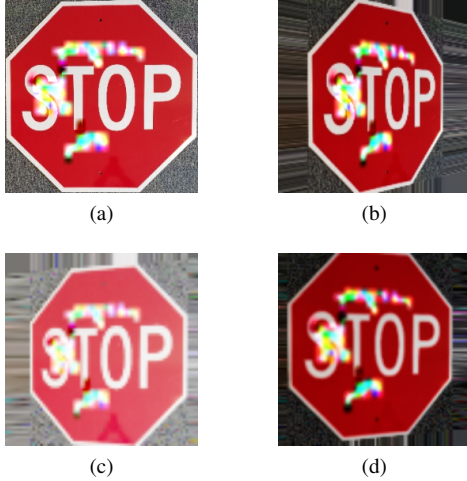


Figure 5. Examples of different transformed images. The upper-left image is the original, and the rest are three examples of transformed versions with perspective, lighting, and blurring transforms.

correction, which applies a nonlinear function. Separately, printers apply nonlinear functions to their colorspace as well. Gamma correction is reflective of nonlinear human sight perception. To model these radiometric-based changes, we model gamma correction under gamma values between  $\frac{1}{\gamma}$  and  $\gamma$ , with half coming from  $[\frac{1}{\gamma}, 1]$  and half coming from  $[1, \gamma]$  in expectation where  $\gamma$  is the maximum gamma value allowed. Assuming the image ranges from  $[0, 1]$ , this is defined as the following:

$$x_{out} = x_{in}^{\gamma} \quad (10)$$

Note that one limitation of gamma correction is that if the color consists of RGB values of 0 or 255, the color does not change regardless of the gamma value.

- 3) **Filtering transformations:** These transformations model changes related to the camera focus. We model Gaussian blurring of different kernel sizes to measure the effects of the target object being out-of-focus. We note that as a side benefit, this may help deal with printer error as some precision in color values is lost in printing. To maximize this printer side benefit, we blur just the perturbation, and let the perspective transform take care of minor out of focus variation in the rest of the image.

We define a single transformation to be a composite function that includes one of each type of modeled transformation. In our case with those listed above, we would have a perspective transform followed by a cropping operation, gamma correction, and a Gaussian blur convolution. Examples of transformed images are shown in Figure 5.

## Appendix C.

### Drive-by Test Images

We include example images from our drive-by experiments in Table 12.

TABLE 12. SAMPLE OF GTSRB DRIVE-BY TEST PICTURES. TOP: SPEED LIMIT 30 KM/HR ATTACK. BOTTOM: PEDESTRIANS ATTACK.



## Appendix D.

### Printing and Lighting Error

We noticed a limitation of gamma correction’s ability to model sun glare and printing errors while testing a Stop Sign to Turn Left Ahead attack. Of particular interest was the discrepancy between the modeled attack’s blues in the digital form and the captured attack’s blues in the physical form.

Examples images for the initial field tests are shown in Table 13 and example images for drive-by tests are shown in Table 14. In the drive-by tests, 42 frames were analyzed and the transform-robustness was 19%.

We can see that the Turn Left Ahead attack is less successful than the Speed Limit 30 km/hr or Pedestrians attack. However, we can easily see that the blue over the “P” is very different in the digital and physical versions, and we hypothesize that it plays a big factor in the performance drop.

To test this hypothesis, we take the outdoor images and digitally darken them. We find that by darkening them we are able to raise the attack success rate from 0% to 52.9%. Likewise, we are also able to increase the attack success rate for the drive-by images by digitally increasing the contrast and decreasing the brightness. This raises the attack success rate from 19% to 47.6%, including successful attacks on the last 11 frames. This suggests that much of the inaccuracy can be attributed to the modeling and error of the blue color.

We can trace this to two limitations printing and lighting error. Printing blue was harder than other colors. In a related issue, a second limitation was the inaccuracies of modeling sun glare, as shown by the increase of attack success in indoor lighting settings (Table 13).

Examining the problem more closely, the color in the blue spot over the “P” includes many instances of the tuple  $(0, 0, 255)$ . While our transforms adjust for lighting with gamma correction, its exponential nature always leaves a tuple like  $(0, 0, 255)$  as  $(0, 0, 255)$ . This suggests a limitation of using gamma correction as a method for modeling lighting changes (especially impact of sunlight) for colors at the extreme ends of the RGB spectrum.

A better model to address lighting changes at extreme ends of the spectrum in EoT transforms may increase

TABLE 13. GTSRB FIELD TEST RESULTS FOR VICTIM STOP SIGN AND TARGET TURN LEFT AHEAD. PHYSICAL ROBUSTNESS RESULTS ARE CALCULATED OVER 5 PICTURES EACH AT THE FOLLOWING SPOTS: 5 FT  $\times$   $\{0^\circ, 15^\circ, 30^\circ, 45^\circ\}$ , 10 FT  $\times$   $\{0^\circ, 15^\circ, 30^\circ\}$ , 15 FT  $\times$   $\{0^\circ, 15^\circ\}$ , 20 FT  $\times$   $\{0^\circ, 15^\circ\}$ , 25 FT, 30 FT, 40 FT. THE ATTACK WAS TESTED 3 TIMES: OUTDOORS, INDOORS WITH INDOOR LIGHTS TURNED OFF, AND INDOORS WITH INDOOR LIGHTS TURNED ON.

Victim	Target	Digital GRAPHITE attack	Physical GRAPHITE attack (outdoors)	Dig. Surv. (100 xforms)	Phys. Surv. (Indoors, lights off)	Phys. Surv. (Indoors, lights on)	Phys. Surv. (Outdoors)
				80%	55.7%	55.7%	0%

TABLE 14. SAMPLE OF GTSRB DRIVE-BY TEST PICTURES FOR TURN LEFT AHEAD ATTACK.



robustness. More accurate modeling of printing error in the transformations could help mitigate this effect as well. We add that we found it difficult to improve the printing quality by adding the NPS term as in  $RP_2$  [18] to GRAPHITE, as oftentimes the limited color palette either made too difficult to find good attacks.

## Appendix E. ALPR Attack

This section includes details on attacking an Automated License Plate Recognition (ALPR) system with GRAPHITE.

### Dataset and Classifiers

For ALPR, we use OpenALPR version 2.3.0, the latest freely available version. We treat this command line tool as a complete black-box. While this particular tool provides confidence info, others may not so we discard that info during our attack. We initialize with the same image but with a gray rectangle filled in with (127, 127, 127) over the plate.

**ALPR Attack Details.** To attack ALPR systems, we imagine printing a license plate holder sticker to cause the ALPR system to fail to detect your license plate number correctly (in an untargeted fashion). In this case, we could attack with just the boosting stage from the (known) border mask consisting of the license plate holder, but this may lead to poor initial transform-robustness. So, we alternate between mask generation and boosting in multiple rounds.

To test our ALPR attack, we print out the license plate holder stickers and place it on expired license plates we acquired for purposes of field testing. We ran ALPR on stationary pictures of the car taken in a driveway and took five pictures of the car at 5', 10', 15', and 20' away at both 0 and 15 degree angles. We generate our attack on images of height 500. The perturbation was generated at a height of 250 and enlarged to fit over the whole image.

As with GTSRB, we use the original author's YOLOv3 [44] object detector network trained on MS COCO [45] to predict bounding boxes for the car. We take the output bounding boxes, crop the sign accordingly, and send the crops to the black-box ALPR pipeline.

**Hyperparameters.** Like our GTSRB attack, we test over  $n = 100$  transformations to compute transform-robustness and take  $q = 10$  gradient samples for RGF sampling [32]. For transformations, we model rotations about the  $y$  axis with homography matrices, lighting changes with gamma correction, and focus changes with Gaussian blurring.

For our ALPR attack, we set rotation to be between  $-15^\circ$  and  $15^\circ$  and fix the base focal length  $f = 10$  ft. We set the Gaussian kernels to sizes 1, 3, and 5, and let the remaining parameters match the GTSRB attack. We used 3 iterations of mask generation and boosting. The patch size for mask generation was  $8 \times 8$ , then  $4 \times 4$ , and then in the last iteration the mask was fixed to just the border. The stride for the patches was the width divided by 2. We additionally added in the backtracking line search to adaptively select the step size as in OPT-attack [20]. We set  $tr_{lo} = 20\%$  and  $tr_{hi} = 60\%$ . We use  $n = 10$  transformations in mask generation and  $n = 50$  transforms in boosting. We set  $\lambda$  in (6) to 25. We do not utilize the  $m_{max}$  option.

**Physical Transform-Robustness Field Tests:** We also evaluate ALPR license plate holder attacks on two plates and cars. In total, we evaluated over 700 physical images.

Table 11 shows ALPR field test results. These attacks took an average of 12950 queries. We found these attacks to have physical success as well. The Washington plate attack success rate was 82.5%. The transform-robustness (digital) for this attack was 80%. 100% of unperturbed, baseline images correctly predicted the license plate. For the Michigan plate attack, the attack succeeded in 67.5% of images while the transform-robustness for this attack was 86%. 82.5% of unperturbed, baseline images correctly predicted the license plate. The average Levenshtein distance, which calculates the number of additions, subtractions, and substitutions required to change one string to another, was 2.175 (including correct predictions). These results also suggest that transform-robustness translates well to physical-world robustness.